

- would be detected, however. We found no evidence of precipitation of iron in the microstructures of our specimens, and believe we would have detected iron had it been present.
- Grains up to 1 mm in diameter are found in native copper [M. Wayman, *CIM Bull.* **78** (no. 880) 67 (1985); *ibid.* **78** (no. 881), p. 75].
 - R. F. Tylecote, in *A History of Metallurgy* (Institute of Metals, London, 1992), pp. 1–11; P. T. Craddock, *Early Metal Mining and Production* (Smithsonian Institution, Washington, DC, 1995), pp. 94–95.
 - Two copper disks were recovered by the University of

Tokyo Expedition from Tomb 5 at Kuntur Wasi, Jequetepeque Valley, in the northern highlands of Peru; the contents of this tomb were dated to the Kuntur Wasi phase (700 to 450 B.C.) [Y. Onuki, Ed., *Kuntur Wasi y Cerro Blanco: Dos Sitios del Formativo en el Norte del Perú* (Hakusen-Sha, Tokyo, 1995), pp. 210–213]. Analysis by Y. Hirao [in (2), p. 30], Table 1, and Fig. 5 identify the metal used as native copper. A copper artifact has also been reported from the Cupisnique cemetery of Puémepe in the lower Jequetepeque Valley, but no technical analysis is available [I. Shimada, in (1), p. 43]. A single sample of copper wire

from the terminal Early Horizon cemetery on the Tablada de Lurín was analyzed by R. Gordon and proved to be made of melted native copper.

- We thank L. Salazar-Burger, J. Pinilla, B. Ojeda, and members of the Proyecto Arqueológico Lurín for support in the field; Peru's Instituto Nacional de Cultura for permission to export the metal samples for analysis at Yale; the Selz Foundation, Heinz Charitable Trust, and the Joseph Fisher Foundation for funding the excavations at Mina Perdida; and Yale's Provostial Research Fund for supporting the laboratory analysis.

7 July 1998; accepted 21 September 1998

Nanoengineering of Inorganic and Hybrid Hollow Spheres by Colloidal Templating

Frank Caruso,* Rachel A. Caruso, Helmuth Möhwald

Hollow silica and silica-polymer spheres with diameters between 720 and 1000 nanometers were fabricated by consecutively assembling silica nanoparticles and polymer onto colloids and subsequently removing the templated colloid either by calcination or decomposition upon exposure to solvents. Scanning and transmission electron microscopy images demonstrate that the wall thickness of the hollow spheres can be readily controlled by varying the number of nanoparticle-polymer deposition cycles, and the size and shape are determined by the morphology of the templating colloid. The hollow spheres produced are envisioned to have applications in areas ranging from medicine to pharmaceuticals to materials science.

In recent years, there has been intense interest surrounding the fabrication of composite micro- and nanoparticles that consist of either organic or inorganic cores coated with shells of different chemical composition (1–8). These core-shell particles often exhibit properties that are substantially different from those of the templated core (for example, different surface chemical composition, increased stability, higher surface area, and different magnetic and optical properties), thus making them attractive from both a scientific and a technological viewpoint. Applications for such particles are diverse, including capsule agents for drug delivery, catalysis, coatings, composite materials, and protecting sensitive agents such as enzymes and proteins. Previous investigations have demonstrated that polymeric microparticles and inorganic cores can be coated with layers of various materials, including silica, yttrium basic carbonate, and zirconium hydrous oxide, either by controlled surface precipitation reactions on the core particles or by direct surface reactions (1–8).

A recently introduced method that allows the construction of composite multilayer assemblies is that of layer-by-layer (LbL) adsorption (9). The basis of the LbL technique is the electrostatic attraction between the charged species deposited (9). Composite multilayers comprising biological macromolecules, multivalent dyes, silicate sheets, or nanoparticles and polymer have been constructed using the LbL approach (9, 10). The buildup of such multilayers has, however, almost exclusively been performed on macroscopically flat substrates (for example, quartz or gold). Recently, the formation of pure polymer multilayers on colloids with the

LbL method has been demonstrated (11). The fabrication of composite, regular inorganic-polymer multilayers on colloidal particles has also been achieved (12), opening the way to the production of novel core-shell materials of given size, topology, and composition. An important extension of core-shell particles is the subsequent removal of the core by either dissolution to produce hollow particles (1–4) or decomposition to give hollow polymer shells (11).

Here we report on the fabrication of hollow inorganic silica and inorganic-hybrid spheres through the colloid templated electrostatic LbL self-assembly of silica nanoparticle (SiO₂)-polymer multilayers, followed by removal of the templated core and, optionally, the polymer (Fig. 1). Polystyrene (PS) latex particles 640 nm in diameter were used as templates, and SiO₂ particles approximately 25 nm in diameter were used as the coating nanoparticles. These nanoparticles electrostatically self-assemble onto the linear cationic polymer poly(diallyldimethylammonium chloride) (PDADMAC) (13). The versatility of the process in forming composite multilayers is demonstrated by the control that can be exerted over the number of deposition cycles, allowing regular uniform multilayers to be formed. Submicrometer-sized hollow spheres, with wall thicknesses ranging from tens to hundreds of nanometers, have been produced. The wall thickness of the hollow spheres and ultimately their shape and stability are dependent on the number of SiO₂-PDADMAC layer deposition cycles (Fig. 1, steps 2 and 3).

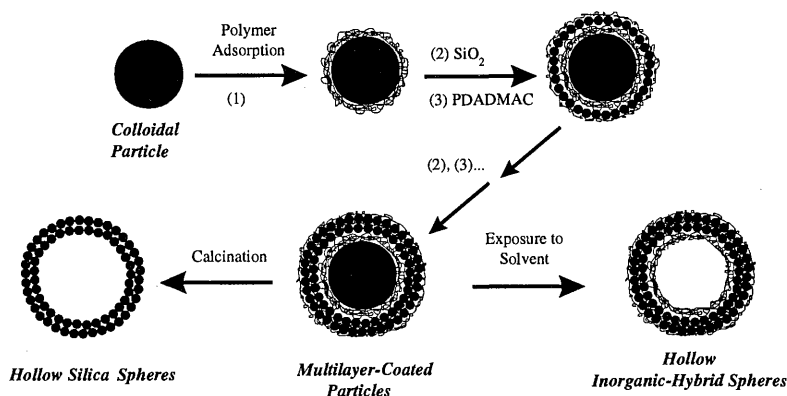


Fig. 1. Illustration of procedures for preparing inorganic and hybrid hollow spheres. The scheme is shown for PS latex particles.

F. Caruso and H. Möhwald, Max Planck Institute of Colloids and Interfaces, Rudower Chaussee 5, D-12489 Berlin, Germany. R. A. Caruso, Max Planck Institute of Colloids and Interfaces, Kantstrasse 55, D-14513 Teltow-Seehof, Germany.

*To whom correspondence should be addressed. E-mail: caruso@mpikg.fta-berlin.de

Table 1. Film thicknesses of the SiO₂-PDADMAC multilayers assembled onto negatively charged PS latex particles, as determined by SPLS. The values were calculated using the Rayleigh-Debye-Gans theory (23) and a refractive index of 1.38. The error in the values is 10%.

Layer number	Multilayer thickness (nm)	
	SiO ₂	SiO ₂ -PDADMAC*
1	25	24
2	70	68
3	117	112
4	169	155
5	210	181

*The decrease in thickness observed when PDADMAC forms the outermost layer is due to the removal of loosely adsorbed SiO₂.

The first step of the hollow sphere fabrication involved the deposition of a three-layer polymer film onto the negatively charged PS latex particles (14). This film provides a smooth and positively charged surface to aid subsequent adsorption of SiO₂ (15). The SiO₂-PDADMAC multilayer films were then formed by the alternate adsorption of SiO₂ and PDADMAC. This method readily permitted control of the composite multilayer film thickness. Regular and uniform SiO₂-PDADMAC multilayer film growth was confirmed by single particle light scattering (SPLS) and transmission electron microscopy (TEM) measurements. The average SiO₂-PDADMAC layer thickness increment calculated from SPLS was 36 nm (Table 1), which is in agreement with the 30 ± 5 nm determined from TEM. The templated PS latex core and polymer were removed after formation of the multilayer film by calcination (that is, by decomposition of the organic matter at 500°C). Alternatively, only the templated core was removed by decomposition in organic solvents.

Scanning electron microscopy (SEM) and TEM micrographs (Fig. 2, A and B) show the presence of SiO₂ nanoparticles on the surface of the PS latex particles (16). Adsorption of a PDADMAC layer on the SiO₂-coated PS latices had the effect of removing loosely adsorbed SiO₂ from the surface and thus reducing the surface roughness and multilayer thickness. Hexagonal packing of the coated particles was observed when they dried. The average particle diameter was 720 ± 10 nm, corresponding to a SiO₂ layer thickness of between 30 and 40 nm (17).

Calcination of PS latices coated with one SiO₂-PDADMAC layer pair (shown in Fig. 2) resulted in hollow spheres composed of silica (Fig. 3) (18). Both broken spheres and complete hollow spheres were obtained. This may indicate that the silica wall thickness was not invariably sufficient to maintain the initial spherical structure of the PS latex particle upon its removal. Alternatively, breakage of the spheres may have been caused by the vacuum in the

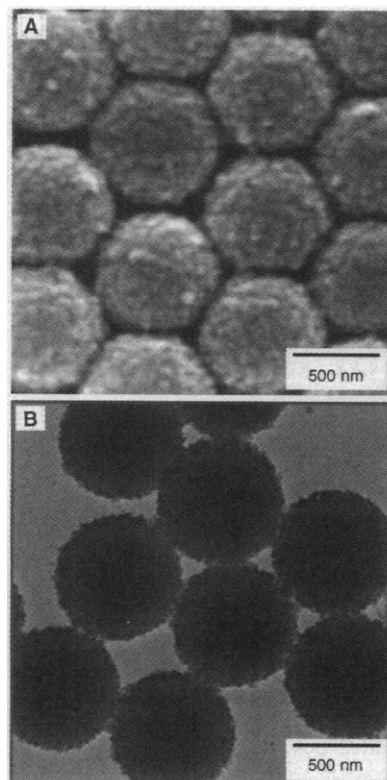


Fig. 2. (A) SEM and (B) TEM micrographs of PS latices coated with one SiO₂-PDADMAC multilayer, showing the SiO₂ nanoparticles on the surface.

SEM (Fig. 3A); most of the hollow spheres imaged by TEM maintained the spherical shape of the templated colloid. The noticeable difference in contrast in the spheres before (Fig. 2B) and after (Fig. 3B) calcination confirms that hollow spheres were produced by the burning off of the organic matter. Thermogravimetric analysis on control samples confirmed the removal of the organic matter during heating to 450°C. Kawahashi and Matijevic also reported total decomposition of PS latices before 500°C (1). The silica nanoparticles can be clearly seen in Fig. 3B. Some particle coalescence (due to siloxane bond formation between free hydroxyl groups) as a result of calcination was observed. The wall thickness, estimated by TEM from the ring around the perimeter of the hollow spheres (Fig. 3B), was approximately 40 ± 10 nm.

The number of SiO₂-PDADMAC multilayers assembled on the PS latices before calcination was found to influence the morphology of the resulting hollow spheres. Complete hollow spheres were obtained when the number of multilayers on the colloids was two or more and the samples were calcined. TEM and SEM micrographs (Fig. 4, B and C) of hollow silica spheres, formed by calcining of PS latices coated with three SiO₂-PDADMAC multilayers, show that the sphericity of the templated particles was preserved. No holes or traces of rupture were identified in these

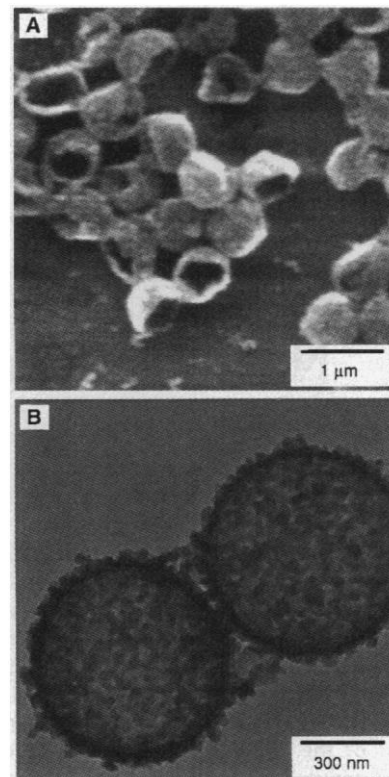


Fig. 3. (A) SEM and (B) TEM micrographs of hollow silica spheres produced by calcination of PS latices coated with one SiO₂-PDADMAC multilayer. Both broken and intact hollow spheres were observed in these samples. The uniformity of the wall thickness can be seen in (B).

samples from the SEM and TEM measurements, which indicates that complete hollow spheres were produced. The spheres were confirmed to be hollow by deliberate application of pressure to break some of them (Fig. 4C) (19). The diameters of the hollow spheres were marginally smaller [by about 5 to 10% (50 to 100 nm)] than those of the corresponding uncalcined (SiO₂-PDADMAC)₃-coated PS latices (Fig. 4A). From Fig. 4, B and C, it is apparent that the walls of the spheres are rather uniform. The sphere wall thicknesses, determined from the TEM images, were approximately 100 ± 15 nm. A tapping-mode atomic force microscopy (AFM) image of a hollow sphere provided information on the morphology of the outer wall of the sphere (Fig. 4D) (20). The surface roughness of the outer surface is due to the silica nanoparticles. In agreement with the TEM data, the AFM image reveals that some silica particle-particle coalescence, as a result of calcination, occurred. AFM measurements of broken hollow spheres clearly showed that the sphere walls were composed of silica particles.

Hollow spheres obtained by calcination of PS latices coated with four or five SiO₂-PDADMAC layers resembled those of the solid, coated PS latices in shape, although

REPORTS

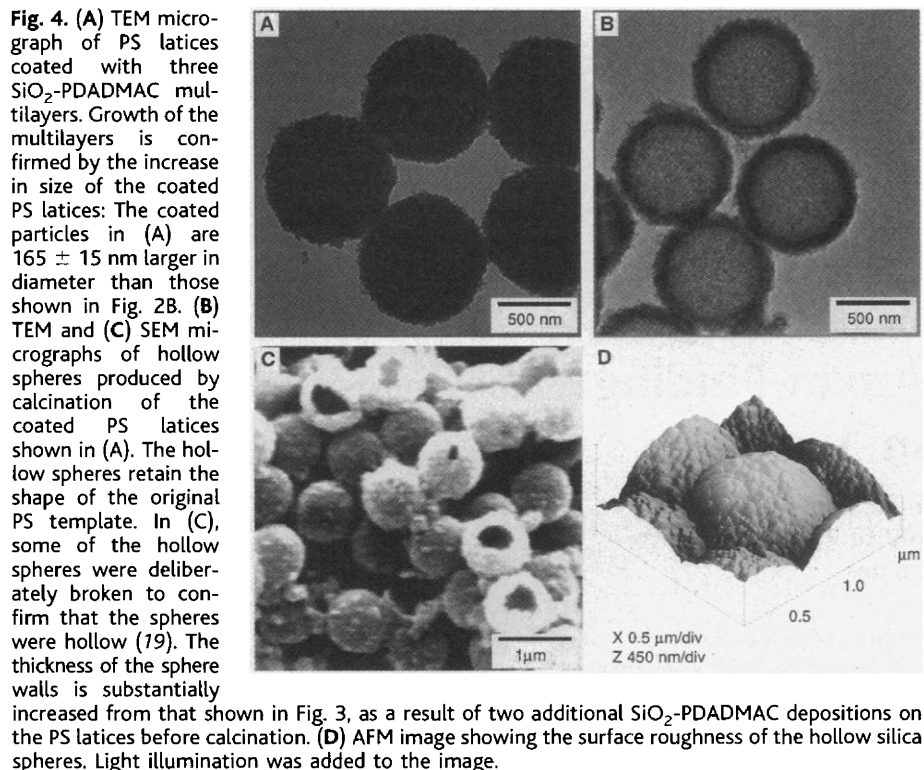


Fig. 4. (A) TEM micrograph of PS latices coated with three SiO_2 -PDADMAC multilayers. Growth of the multilayers is confirmed by the increase in size of the coated PS latices: The coated particles in (A) are 165 ± 15 nm larger in diameter than those shown in Fig. 2B. (B) TEM and (C) SEM micrographs of hollow spheres produced by calcination of the coated PS latices shown in (A). The hollow spheres retain the shape of the original PS template. In (C), some of the hollow spheres were deliberately broken to confirm that the spheres were hollow (19). The thickness of the sphere walls is substantially increased from that shown in Fig. 3, as a result of two additional SiO_2 -PDADMAC depositions on the PS latices before calcination. (D) AFM image showing the surface roughness of the hollow silica spheres. Light illumination was added to the image.

their diameter was slightly reduced. SEM examination of intentionally broken spheres revealed that the wall thickness was directly related to the number of SiO_2 -PDADMAC deposition cycles: An increase of 30 to 40 nm in the wall thickness of the hollow spheres was observed for each additional SiO_2 -PDADMAC layer deposited onto the PS latices before calcination.

The templated PS latex core could also be removed by exposure of the SiO_2 -PDADMAC-coated particles to tetrahydrofuran, allowing the production of composite silica-polymer hollow spheres. Swelling of the PS colloid before decomposition ruptured the SiO_2 -polymer coating, resulting in broken hollow spheres when the wall was only one or two silica layers thick. Intact hollow spheres were obtained when the sphere wall thickness was increased. The use of a different colloidal core, such as weakly cross-linked melamine-formaldehyde (MF) particles (11), permitted the core to be removed by exposure of the coated particles to either acidic solutions ($\text{pH} < 1.6$) (11) or dimethylsulfoxide, leaving behind silica-polymer hollow spheres. No substantial swelling of the MF particles occurred before their decomposition, therefore avoiding rupturing of the walls. The oligomers produced upon MF particle decomposition consist mostly of 5 to 10 monomers, thereby readily permeating the multilayers and allowing their removal (11, 21). Spherical MF particles 3 μm in diameter have also been successfully used as templates for SiO_2 -PDADMAC multilayer buildup, producing micrometer-sized, hollow silica spheres upon cal-

ination. This shows that larger-size templating colloids can also be used.

It has been demonstrated that the LbL self-assembly technique, when applied to produce composite SiO_2 nanoparticle-polymer multilayers on colloids, coupled with removal of the core (and optionally the polymer), provides a successful pathway for fabricating inorganic and inorganic-hybrid hollow spheres in the sub-micrometer-to-micrometer size range. Important advantages of this method of fabricating hollow spheres are as follows: (i) the thickness of the hollow sphere walls can be readily controlled by varying the number of deposition cycles; (ii) the size and shape of the spheres produced are determined by the dimensions of the templating colloid employed; (iii) the method is generally applicable to a wide variety of charged inorganic particles, thereby making possible the production of various inorganic (such as TiO_2 and ZrO_2) and composite (magnetic nanoparticle and SiO_2 or TiO_2) hollow spheres.

Preliminary experiments have shown that the technique described above can be used to make hollow spheres of other inorganic materials (TiO_2) and various nanocomposite (inorganic-hybrid and inorganic-inorganic) hollow spheres, as well as hollow shells from templated biological specimens (22).

References and Notes

1. N. Kawahashi and E. Matijevic, *J. Colloid Interface Sci.* **143**, 103 (1991).
2. M. Giersig, T. Ung, L. M. Liz-Marzan, P. Mulvaney, *Adv. Mater.* **9**, 570 (1997); M. Giersig, L. M. Liz-Marzan, T.

- Ung, D. S. Su, P. Mulvaney, *Ber. Bunsenges. Phys. Chem.* **101**, 1617 (1997).
3. H. Barnholker, B. Nitzan, S. Gura, S. Margel, *J. Mater. Sci. Lett.* **16**, 1412 (1997).
4. D. Walsh and S. Mann, *Nature* **377**, 320 (1995).
5. A. Garg and E. Matijevic, *J. Colloid Interface Sci.* **126**, 243 (1988); N. Kawahashi and E. Matijevic, *ibid.* **138**, 534 (1990); M. Ohmori and E. Matijevic, *ibid.* **150**, 594 (1992).
6. L. M. Liz-Marzan, M. Giersig, P. Mulvaney, *Langmuir* **12**, 4329 (1996); *J. Chem. Soc. Chem. Commun.* (1996), p. 731; M. A. Correa-Duarte, M. Giersig, L. M. Liz-Marzan, *Chem. Phys. Lett.* **286**, 497 (1998).
7. S. Margel and E. Weisel, *J. Polym. Sci. Chem. Ed.* **22**, 145 (1984).
8. A. P. Philipse, M. P. B. van Bruggen, C. Pathmamanoharan, *Langmuir* **10**, 92 (1994).
9. G. Decher, *Science* **277**, 1232 (1997) and references therein; G. Decher and J.-D. Hong, *Makromol. Chem. Macromol. Symp.* **46**, 321 (1991).
10. F. Caruso, K. Niikura, D. N. Furlong, Y. Okahata, *Langmuir* **13**, 3427 (1997); Y. Lvov, K. Ariga, M. Onda, I. Ichinose, T. Kunitake, *ibid.*, p. 6195; E. R. Kleinfield and G. S. Ferguson, *Science* **265**, 370 (1994); G. B. Sukhorukov, H. Möhwald, G. Decher, Y. M. Lvov, *Thin Solid Films* **285**, 220 (1996); Y. Lvov, K. Ariga, T. Kunitake, *J. Am. Chem. Soc.* **117**, 6117 (1995); S. W. Keller, S. A. Johnson, E. S. Bringham, E. H. Yonemoto, T. E. Mallouk, *ibid.*, p. 12879; Y. L. Liu, M. Q. Zao, D. E. Bergbreiter, R. M. Crooks, *Angew. Chem. Int. Ed.* **36**, 2114 (1997).
11. E. Donath, G. B. Sukhorukov, F. Caruso, S. A. Davis, H. Möhwald, *Angew. Chem. Int. Ed.* **37**, 2201 (1998); G. B. Sukhorukov et al., *Polym. Adv. Technol.* **9**, 1 (1998).
12. F. Caruso, H. Lichtenfeld, M. Giersig, H. Möhwald, *J. Am. Chem. Soc.* **120**, 8523 (1998).
13. The solution pH was adjusted to between 5 and 6 so that the SiO_2 nanoparticles (Ludox TM40, Dupont) were negatively charged and PDADMAC (Aldrich, molecular weight $< 200,000$) was positively charged. The SiO_2 nanoparticles have an isoelectric point of about 3.
14. The precursor polyelectrolyte layers [PDADMAC/poly(styrenesulfonate, sodium salt) (PSS)/PDADMAC] were consecutively deposited onto the negatively charged sulfate-stabilized PS latices from 1 mg ml^{-1} polyelectrolyte solutions containing 0.5 M NaCl, with an adsorption time of 20 min. SiO_2 nanoparticles were subsequently deposited by exposing the polyelectrolyte-coated PS latices to a 2 weight % SiO_2 suspension in 0.1 M NaCl ($\text{pH} \sim 5$ to 6) for 15 min. In each step, nonadsorbed polyelectrolyte or SiO_2 was removed by four repeated centrifugation (13500g)/water wash/redispersion cycles.
15. Electrophoretic mobility measurements yielded a zeta potential of approximately 50 mV for the [PDADMAC/PSS/PDADMAC]-coated PS particles.
16. SEM measurements were performed with a Zeiss DSM 940 instrument operated at an accelerating voltage of 20 kV. SEM samples (on carbon or quartz surfaces) were coated with about 5 nm of Pd or Au. TEM images were recorded on a Phillips CM12 microscope operating at 120 kV. Samples for TEM were sonicated in water for 1 min (to redisperse the hollow spheres) and subsequently deposited onto a carbon grid.
17. The thickness of the precursor polyelectrolyte layers on the PS latices is approximately 5 nm; that is, the average diameter of the coated particles before SiO_2 deposition is approximately 650 nm. The PDADMAC layer thickness accounts for at most only 2 nm of the total multilayer (SiO_2 -PDADMAC) film thickness.
18. Silica and inorganic-hybrid hollow spheres were produced by drying the sample of PS latices coated with SiO_2 -PDADMAC multilayers on aluminum sheets or quartz slides at room temperature and then calcining (heating rate, 5 K min^{-1}) at 500°C under N_2 for 4 hours and a further 8 hours under O_2 .
19. Only intact, complete shells were imaged on aluminum substrates. However, broken shells were observed solely in samples that were transferred from aluminum (on which they were calcined) to carbon surfaces for SEM analysis. The breakage was a result of pressure applied during the transfer by scraping with a metal object or by pressing the calcined sample on the carbon surface to effect transfer of the

- spheres. No other differences were observed between samples imaged on aluminum or carbon surfaces.
20. AFM images were obtained with a Digital Instruments Nanoscope IIIa AFM in tapping mode. Samples were deposited onto quartz slides.
21. Monomeric molecules with dimensions of 1 to 2 nm can readily permeate multilayer films [see F. Caruso, E.

- Donath, H. Möhwald, *J. Phys. Chem. B* **102**, 2011 (1998); R. v. Klitzing and H. Möhwald, *Macromolecules* **29**, 6901 (1996)].
22. F. Caruso, R. A. Caruso, H. Möhwald, unpublished results.
23. M. Kerker, *The Scattering of Light and Other Electromagnetic Radiation* (Academic Press, New York, 1969).

24. F.C. acknowledges the Alexander von Humboldt Foundation for support in the form of a research fellowship. We thank J. Hartmann for assistance with preliminary SEM measurements and M. Giersig for use of the TEM.

15 July 1998; accepted 6 October 1998

Auxin-Dependent Cell Expansion Mediated by Overexpressed Auxin-Binding Protein 1

Alan M. Jones,* Kyung-Hoam Im, Michael A. Savka,†
Ming-Jing Wu, N. Gregory DeWitt, Raymond Shillito,
Andrew N. Binns

To test the hypothesis that auxin-binding protein 1 (ABP1) is a receptor controlling auxin-mediated plant cell expansion, *ABP1* complementary DNAs were expressed in a controllable fashion in tobacco plants and constitutively in maize cell lines. Induction of *Arabidopsis ABP1* expression in tobacco leaf strips resulted in an increased capacity for auxin-mediated cell expansion, whereas induction of *ABP1* in intact plants resulted in leaves with a normal morphology, but larger cells. Similarly, constitutive expression of maize *ABP1* in maize cell lines conferred on them the capacity to respond to auxin by increasing cell size. These results support a role of *ABP1* as an auxin receptor controlling plant growth.

Auxins are plant growth hormones that cause rapid increases in plant cell wall extensibility, alter ion flux at the plasma membrane, and cause specific changes in gene expression (1, 2). A receptor mediating these effects has not been unequivocally identified, although *ABP1* is a leading candidate for at least the plasma membrane and wall effects (1). *ABP1* has been carefully characterized with regard to its auxin-binding properties (3). Moreover, it has been shown to fit the criteria of a receptor mediating auxin-induced cell expansion, on the basis of its expected tissue distribution, its plasma membrane location, and on results from experiments designed to antagonize or mimic auxin action using antibodies to *ABP1* and an *ABP1* peptide mimetic (4, 5). These results, while consistent with *ABP1* receptor function, are nonetheless indirect. Therefore, we took a molecular genetic approach by examining the effect of inducible overexpression of *ABP1* in plants and

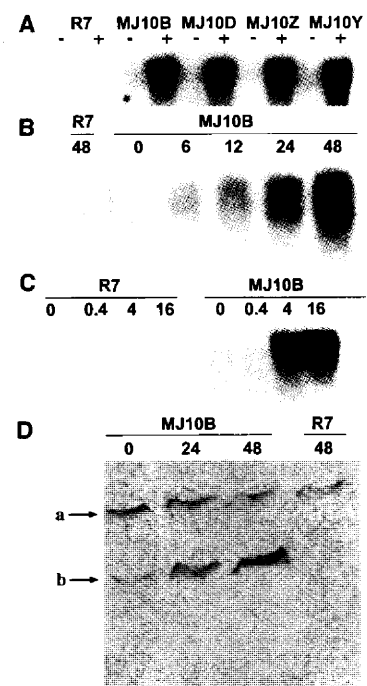
constitutive expression in cell lines.

Tobacco plants expressing the tetracycline repressor were transformed with the full-length, *Arabidopsis ABP1* cDNA placed under the control of a tetracycline promoter (6). The inducible expression of *ABP1* in these plants is

Fig. 1. Anhydrotetracycline-inducible expression of *ABP1* in tobacco. **(A)** Northern blot analysis of *Arabidopsis ABP1* transcript level in total RNA (15 μ g) isolated from all leaves of 40-day-old (3 to 4 leaf stage) control plants (R7, expressing the tetracycline repressor) and four independently transformed tobacco plants (MJ10B, MJ10D, MJ10Z, MJ10Y) expressing both the tetracycline repressor and the tet-inducible *Arabidopsis ABP1* construct. Plants were hydroponically fed 12 μ g/ml of the nontoxic tetracycline analog AhTet via the roots for 48 hours (+) or left untreated (-) on the lab bench under 10/14 light/dark cycles at 25°C. **(B)** Northern blot analysis of the *Arabidopsis ABP1* transcript level in total RNA from R7 and MJ10B tobacco plants after the indicated number of hours in the presence of 12 μ g/ml of AhTet. **(C)** Northern blot analysis of the *Arabidopsis ABP1* transcript level in total RNA from R7 and MJ10B tobacco plants after 48 hours treatment with AhTet at the indicated concentrations (micrograms per milliliter). **(D)** Protein immunoblot analysis of *Arabidopsis ABP1* in crude microsomal fractions from R7 and MJ10B tobacco plants after the indicated hours of treatment with 4 μ g/ml of AhTet. MJ10B plants are homozygous for the *Arabidopsis ABP1* transgene. Polyclonal antisera directed against recombinant *Arabidopsis ABP1* were used. Note that this serum does not recognize tobacco *ABP1* (lane R7, 48 hours). Band "b" represents the *Arabidopsis ABP1*. The nonspecific recognition of band "a" shows equal loading between the samples.

shown in Fig. 1A. One transformant designated MJ10B was used to further characterize the induction kinetics and dose dependence of induction (Fig. 1, B and C). Steady-state transcript is detectable in uninduced transformants and is shown to greatly increase within 6 hours after application of anhydrotetracycline (AhTet). *Arabidopsis ABP1* protein (7) is detected by immunoblot analysis in uninduced MJ10B transformants (homozygous for *ABP1* transgene) and increases significantly during the 48 hours after induction (Fig. 1D).

Having established the transgene induction kinetics and expression characteristics, we began our analysis of the physiological effect of ectopic expression of *ABP1* in leaves, because previous work found that *ABP1* mediates auxin-induced hyperpolarization in mesophyll protoplasts. The capacity of leaf cells to respond to auxin is developmentally acquired (8). Cells in the tips of young leaves respond to auxin by ethylene-independent expansion, whereas cells in the base of the lamina do not acquire this capacity until much later as the basal lamina expands. We therefore chose to examine the effect of controlled expression of *ABP1* in cells of the basal region of the lamina at a time point when they are not normally auxin responsive. Interveneal lamina tissue taken from the basal region of *ABP1* transformants exhibited AhTet-



A. M. Jones, K.-H. Im, M.-J. Wu, N. G. DeWitt, Department of Biology, University of North Carolina, Chapel Hill, NC 27599-3280, USA. M. A. Savka and A. N. Binns, Department of Biology, University of Pennsylvania, Philadelphia, PA 19104-6018, USA. R. Shillito, Agricultural Research Center, AgrEvo USA, Pikeville, NC 27863, USA.

*To whom correspondence should be addressed. E-mail: alan_jones@unc.edu

†Present address: Department of Biology, University of West Florida, Pensacola, FL 32514, USA.